Marquette University

e-Publications@Marquette

Physics Faculty Research and Publications

Physics, Department of

Direct Evidence That the Reaction Intermediate of Metallo-**β**-lactamase L1 Is Metal Bound

James D. Garrity
Miami University - Oxford

Brian Bennett
Marquette University, brian.bennett@marquette.edu

Michael W. Crowder
Miami University - Oxford

Direct Evidence That the Reaction Intermediate of Metallo-β-lactamase L1 Is Metal Bound

James D. Garrity
Department of Chemistry and Biochemistry, Miami University, Oxford, Ohio
Brian Bennett
National Biomedical EPR Center, Department of Biophysics, Medical College of Wisconsin, Milwaukee, Wisconsin
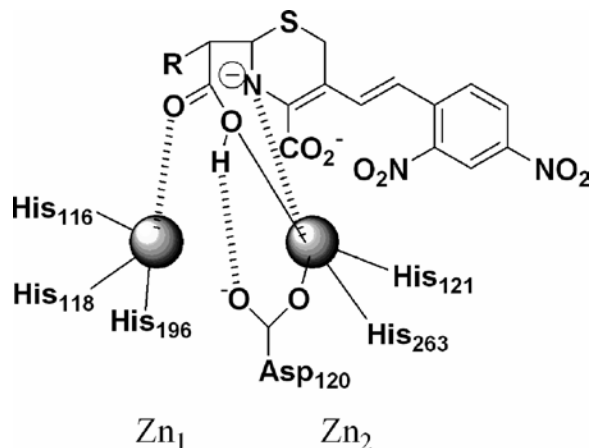Michael W. Crowder
Department of Chemistry and Biochemistry, Miami University, Oxford, Ohio

SUBJECTS:
Kinetic parameters, Peptides and proteins, Metals, Ions

Abstract

In an effort to probe the structure of the reaction intermediate of metallo-β-lactamase L1 when reacted with nitrocefin and other β-lactams, time-dependent absorption and rapid-freeze-quench (RFQ) EPR spectra were obtained using the Co(II)-substituted form of the enzyme. When using nitrocefin as the substrate, time-dependent absorption spectra demonstrate that Co(II)-substituted L1 utilizes a reaction mechanism, similar to that of the native Zn(II) enzyme, in which a short-lived intermediate forms. RFQ-EPR spectra of this intermediate demonstrate that the binding of substrate results in a change in the electronic properties of one or both of the Co(II)'s in the enzyme that is consistent with a change in the coordination sphere of this metal ion. This observation provides evidence that the reaction intermediate is a metal-bound species. RFQ-EPR studies also demonstrate that other β-lactams, such as cephalothin, meropenem, and penicillin G, proceed through an electronically similar complex and that the role of metal is similar in all cases. EPR spectroscopy has also identified distinct product-bound species of L1, indicating that reversible product binding must be considered in all future kinetic mechanisms. Consideration of the time-dependent optical and EPR studies in light of available crystallographic information indicates the intimate involvement of the metal ion in the Zn_2-binding site of L1 in the hydrolytic reaction.

The ability of bacteria to acquire resistance to antibiotics is a serious problem that continues to challenge modern society (*1*). Excessive use, and often misuse, of antibiotics in the clinic and for agricultural purposes has resulted in tremendous selective pressure for antibiotic-resistant bacteria (*2*). These bacteria utilize a variety of methods to become resistant, including modification of cell wall components to prevent antibiotic binding, expression of efflux pumps that transport the antibiotic out of the cell, and the production of enzymes that modify and render antibiotics ineffective (*1, 2*).

The most common, least expensive, and effective antibiotics currently used are the β-lactams, such as carbapenems, cephalosporins, and penicillins (*3, 4*). These antibiotics are mechanism-based inhibitors of transpeptidase, a bacterial enzyme required for the production of a strong, viable cell wall (*5, 6*). In response to their widespread use, an increasing number of bacterial strains have acquired the ability to produce β-lactamases, enzymes that hydrolyze and render β-lactam antibiotics ineffective. There are over 300 distinct β-lactamases known, and Bush has classified these into four distinct groups on the basis of their molecular properties (*5, 6*). One of the more troubling of these is group 3, the metallo-β-lactamases, which are Zn(II)-dependent enzymes that hydrolyze nearly all known β-lactams and for which there are no clinically useful inhibitors (*7–14*). To date, there are no reports of a metallo-β-lactamase being isolated from a major pathogen (*15, 16*); however, these enzymes are produced by a variety of minor clinical pathogens such as *Bacteroides fragilis*, *Pseudomonas aeruginosa*, and *Stenotrophomonas maltophilia*, and the continued extensive use of β-

lactam-containing antibiotics will inevitably result in the production of a metallo-β-lactamase by a major pathogen (*2*).

There is significant diversity within the metallo-β-lactamases, and Bush, on the basis of their amino acid sequence identities and substrate affinities, has further divided them into three subgroups (*17*). A similar grouping scheme based on structural properties has also been offered (*18*). The diversity of these subgroups is best exemplified by their vastly differing efficacies toward nonclinical inhibitors; these differences lead to the prediction that finding a single inhibitor for all metallo-β-lactamases may not be possible (*14, 19–27*. To address this problem, we are currently characterizing a representative enzyme from each of the metallo-β-lactamase subgroups with the goal of identifying common structural and mechanistic similarities that can be targeted for the generation of clinically useful inhibitors. This work describes our efforts on metallo-β-lactamase L1 from *S. maltophilia* (L1).[1]

S. maltophilia is an important pathogen in nosocomial infections of immunocompromised patients suffering from cancer, cystic fibrosis, drug addition, and AIDS and in patients with organ transplants and on dialysis (*28–30*). This organism is inherently resistant to most antibiotics due to its low outer membrane permeability (*31*) and is particularly resistant to β-lactams due to the production of a chromosomally expressed group 2e β-lactamase (L2) and a group 3c β-lactamase (L1) (*32, 33*). L1 has been cloned, overexpressed, and partially characterized by kinetic and crystallographic studies (*34, 35*). The enzyme exists as a homotetramer of ca. 118 kDa in solution and in the crystalline state, tightly binding two Zn(II) ions per subunit. The Zn_1 site has three histidine residues and one bridging hydroxide as ligands, and the Zn_2 site has two histidines, one aspartic acid, one terminally bound water, and the bridging hydroxide as ligands (Figure 1).
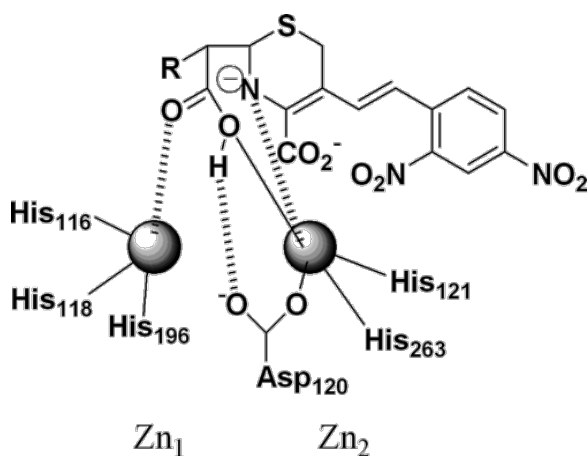

Figure 1 Proposed metal binding site of metallo-β-lactamase L1 when bound to the reaction intermediate. Figure rendered with CS ChemDraw Ultra version 5.0.

Efforts to solve the crystal structure of one of the metallo-β-lactamases with a bound substrate molecule have failed, most likely due to the high activity of the enzymes, even in the crystalline state, toward all β-lactam-containing antibiotics (*35, 36*). Therefore, computational studies have been used extensively to provide insight into substrate binding, the role of the Zn(II) ions in catalysis, the protonation state of the active site, protein dynamics, and inhibitor binding (*35, 37–42*.

Previous studies on metallo-β-lactamase CcrA from *B. fragilis* (*43*) and L1 (*44, 45*) have led to proposals for a mechanism of catalytic hydrolysis in which intermediates in catalysis may be stabilized by the active site metal ions (*43, 46*). In the present work, we demonstrate that a chromophoric, substrate-derived species is formed within a kinetically relevant time. We also show that the electronic structures of the catalytic metal ions are perturbed concomitantly with formation of this intermediate species. For the first time, direct evidence for the

involvement of the metal ions in non-rate-limiting formation of a catalytic cycle intermediate is presented. Further insight into the catalytic mechanism is gleaned from studies with three classes of substrate.

Experimental Procedures

Escherichia coli strains DH5α and BL21(DE3) were obtained from Gibco-BRL and Novagen, respectively. The plasmid pET26b was purchased from Novagen. Luria–Bertani (LB) media in powder form were purchased from Gibco-BRL. Isopropyl β-thiogalactoside (IPTG), biotech grade, was procured from Anatrace. Protein solutions were concentrated with an Amicon ultrafiltration cell equipped with YM-10 DIAFLO membranes from Amicon, Inc. Dialysis tubing was prepared using Spectra/Por regenerated cellulose molecular porous membranes with a molecular weight cutoff of 6000–8000 (*47*). Q-Sepharose Fast Flow was purchased from Amersham Pharmacia Biotech. 1,10-Phenanthroline was purchased from Sigma. Nitrocefin was purchased from Becton Dickinson, and solutions of nitrocefin were filtered through a Fisherbrand 0.45 μm syringe filter (*34*). Cephalothin and penicillin G were purchased from Sigma and Fisher, respectively. Meropenem was generously supplied by Zeneca Pharmaceuticals. Ring-opened analogues of the antibiotics were prepared by adding catalytic amounts of L1 to concentrated solutions of the antibiotic and allowing the reactions to proceed to completion. All buffers and media were prepared using Barnstead NANOpure ultrapure water.

Large-scale (4 L) preparations of the L1 were performed as described previously (*34*). Protein purity was ascertained by SDS–PAGE. Purified protein was dialyzed versus 6 × 1 L of 50 mM HEPES, pH 7.0, with 5 mM 1,10-phenanthroline, over 36 h at 4 °C, followed by dialysis versus 6 × 1 L of metal-free 50 mM HEPES, pH 7.0, over 36 h at 4 °C, to yield apo-L1. Two equivalents of Co(II) was added per apo-L1 monomer using published methods (*48*). Co(II) incorporation was confirmed by comparing the EPR spectra of Co(II)-L1 and HEPES buffer containing 1 mM Co(II). The spectra were quite distinguishable, and there was no evidence for Co(II)-HEPES in the Co(II)-L1 samples.

Time-dependent spectrophotometric studies of nitrocefin hydrolysis by Co(II)-substituted L1 were performed on an Applied Photophysics SX.18MV stopped-flow spectrophotometer, as previously described (*49, 50*).

Samples for EPR studies were generated using a modified Update Instruments (Madison, WI) rapid-freeze-quench (RFQ) system. All enzyme and substrate starting sample concentrations were 1 mM (except penicillin G which was 4 mM), prepared in metal-free (Chelex 100, Bio-Rad) 50 mM HEPES, pH 7.0. A model 715 Update Instruments ram controller was used to drive a PMI-Kollmorgen stepping motor (model 010-00205-010) connected to a ram that in turn drove the Update Instrument syringes. The syringes, mixer, and tubing were all contained in a watertight bath that was maintained at 2 °C using iced water. Immediately prior to sample collection, the nozzle (and, for the shortest reaction times, the attached mixer) was removed from the bath and held 5 mm above the surface of 2-methylbutane (Fisher) contained in a collecting funnel and maintained at −130 °C by a surrounding bath (Update Instruments) of liquid nitrogen cooled 2-methylbutane. Samples were packed into EPR tubes at −130 °C, excess 2-methylbutane was decanted, and samples were stored in liquid nitrogen prior to EPR examination, typically within 1 h of sample generation. The RFQ system was calibrated by comparing the development of a low-spin Fe(III) EPR signal and the disappearance of a high-spin Fe(III) EPR signal with the associated optical changes at 636 nm using stopped-flow spectrophotometry, upon mixing myoglobin with an excess of sodium azide. The shortest, total effective reaction time that could be achieved with the RFQ system was 10 ms.

EPR spectra were recorded using a Bruker EleXsys E500 EPR spectrometer equipped with an Oxford Instruments ITC4 temperature controller and an ESR-900 helium flow crystat. Spectra were recorded at 12 K with 1 mW microwave power. A Bruker ER-4116DM cavity was used, with a resonant frequency of 9.63 GHz (in perpendicular mode), and 10 G (1 mT) field modulation at 100 kHz was employed. Computer simulations of EPR

spectra were carried out using the matrix diagonalization program XSophe [Bruker Biospin GmbH (*51*)] assuming a spin Hamiltonian $\mathcal{H}$ = β**gBS + SDS**, where $S = {}^3/_2$ and $D > 0$ corresponds to an $M_S = |\pm^1/_2\rangle$ ground state Kramers' doublet. For Co(II), generally $|D| \gg \beta gBS$, and the spectrum is therefore insensitive to the precise value of D; in this work the arbitrary value D = 50 cm^{-1} was taken. The **g** tensor was assumed to have at least axial symmetry as this allows for a unique solution to the spin Hamiltonian in terms of the real g-values, g_z and g_{xy} (or $g_\parallel$ and $g_\perp$), and the rhombic distortion of the axial zero-field splitting, E/D (*52*). The relationship between the resonance positions, $g_{\mathrm{eff}(x,y,z)}$, and these parameters is described in detail elsewhere (*53, 54*). Line widths were simulated using a single strain parameter for each of the principal orientations. Where simulations of spectra are shown that contain more than one species, spectra that could be well simulated assuming a single set of spin Hamiltonian parameters were used as basis spectra, and linear combinations of two (and no more than two) basis spectra were used to model the spectra collected after reaction times intermediate between those after which the basis spectra were recorded. Contributions of the individual species are estimated as ±5% of the total spins.

Results

Stopped-Flow Spectrophotometric Studies on Co(II)-Substituted L1.

L1 has been reported to exhibit a steady-state k_{cat} of 41 s^{-1} at 25 °C with nitrocefin as the substrate. Previous stopped-flow studies have shown that progress of the reaction of L1 with nitrocefin is sufficiently rapid that stopped-flow techniques at 25 °C may not access the entire catalytic cycle (*44, 45, 50*). Pre-steady-state kinetic studies were therefore conducted at both 2 and 25 °C. Although only a few data points could be collected for the initial phase of the reaction of L1 with nitrocefin at 25 °C, time-dependent spectrophotometry at 2 and 25 °C indicated that the course of the reaction at both temperatures was indistinguishable except for the proportionally lower rate constants for each step at the lower temperature. Studies at 2 °C on the reaction of 100 µM Zn(II)-containing L1 with 100 µM nitrocefin revealed the time-dependent presence of three distinct species: (1) at 7 ms after mixing, there was a small feature at 390 nm corresponding to substrate nitrocefin and a large feature at 665 nm that was previously assigned to a reaction intermediate (*45*), (2) at 36 ms after mixing, the feature at 665 nm was slightly less intense and exhibited a shoulder at 485 nm, and (3) at 1 s, the features at 390 and 665 nm were absent, and a feature, which corresponds to product, at 485 nm was observed (Figure 2A). Single wavelength versus time plots (Figure 2B) of the features at 390, 485, and 665 nm were similar in appearance to those previously reported and were individually fitted to exponential equations as described in McMannus et al. (*45*). The decay of substrate (feature at 390 nm) was found to occur at a rate constant of 269 ± 7 s^{-1}, which was similar to the rate constant of intermediate (feature at 665 nm) formation (250 ± 5 s^{-1}). The breakdown of the 665 nm intermediate occurred at a rate constant of 7.3 ± 0.1 s^{-1}, which corresponded to the rate constant of product formation (feature at 485 nm) of 7.6 ± 0.1 s^{-1}. These rate constants support the conclusion that the same mechanism that was predicted for L1 at 25 °C operates at 2 °C.
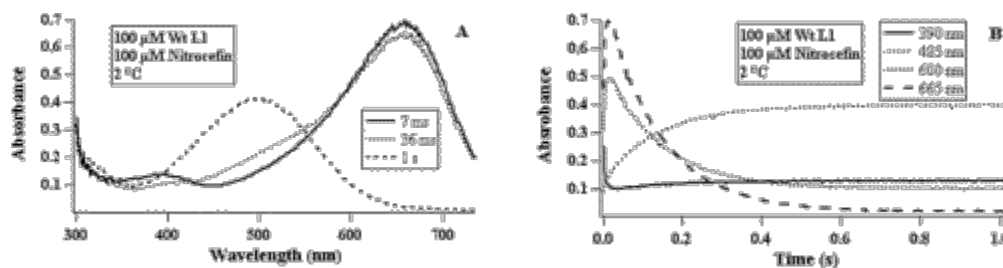
Figure 2 (A) Rapid-scanning electronic absorption spectra of the reaction of 100 µM wild-type L1 with 100 µM nitrocefin at 2 °C. (B) Single wavelength versus time plots of the reaction of 100 µM wild-type L1 with 100 µM nitrocefin at 2 °C. The buffer used in both reactions was 50 mM HEPES, pH 7.0.

Stopped-flow spectrophotometry at 2 and 25 °C indicated that the course of the reaction between Co(II)-substituted L1 and nitrocefin was also indistinguishable at both temperatures, apart from the proportionally lower rate constants for each step at the lower temperature. Time-dependent absorption spectra recorded at 2 °C of Co(II)-substituted L1 with nitrocefin as the substrate showed the same three species that were observed in the studies with Zn(II)-L1. However, at 36 ms, the intermediate at 665 nm converts to a fourth species that absorbs at 600 nm, and this second intermediate then is converted into product (Figure 3A). Single wavelength versus time plots of these data were individually fitted to exponential equations (Figure 3B). Substrate decay (390 nm) occurred at a rate constant of 67 ± 2 s^{-1}, which is similar to the rate constant of formation of the 665 nm intermediate (rate constant = 54 ± 3 s^{-1}) and of the 600 nm intermediate (rate constant = 72 ± 2 s^{-1}). The breakdown of both intermediates occurred at rate constants of 7.0 ± 0.1 s^{-1} (665 nm feature) and 6.7 ± 0.1 s^{-1} (600 nm feature), which is similar to the rate constant of product formation of 8.8 ± 0.1 s^{-1}.
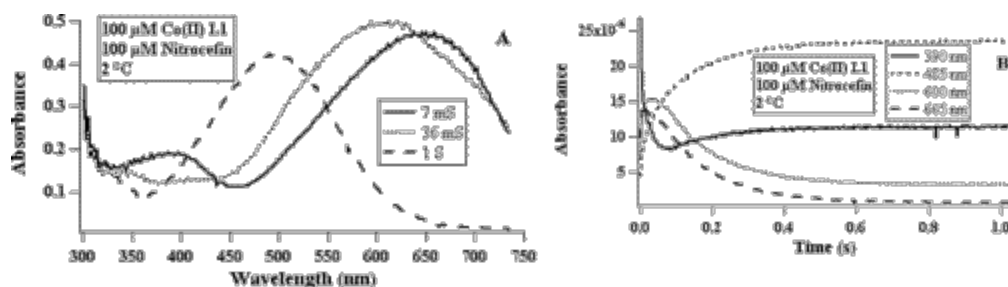

Figure 3 (A) Rapid-scanning electronic absorption spectra of the reaction of 100 µM Co(II)-substituted L1 with 100 µM nitrocefin at 2 °C. (B) Single wavelength versus time plots of the reaction of 100 µM Co(II)-substituted L1 with 100 µM nitrocefin at 2 °C. The buffer used in both reactions was 50 mM HEPES, pH 7.0.

The possibility that the mechanism of Co(II)-L1 may be different from that of Zn(II)-L1 was considered. In particular, the possibility was explored that the appearance of a chromophoric intermediate with Co(II)-L1 was not observed with Zn(II)-L1, suggestive of a branched mechanism (55, 56). Such a mechanism would exhibit an initial burst phase in pre-steady-state kinetics, with a burst amplitude greater than the concentration of the enzyme (55, 56). However, no pre-steady-state burst could be detected in stopped-flow spectrophotometric experiments. Kinetic simulations of our data suggest a linear mechanism with multiple intermediates (Scheme 1), one or more of which are as yet uncharacterized. This complex mechanism may be in operation with Zn(II)-L1 as well as with Co(II)-L1. If, as we propose, the intermediates are metal-bound, then the electronic structure of the metal ion would influence the energies of the electronic absorption transitions observed for the 600 and 665 nm intermediates with Co(II). It is entirely possible that although these transitions are just resolvable in Co(II)-L1, these transitions overlap sufficiently in Zn(II)-L1 that the absorption bands are not resolved. Temporal resolution of two spectrophotometrically indistinguishable intermediates is not possible in the studies with Zn-L1: with Co(II)-L1, the kinetics of formation and decay of the 600 and 665 nm species are only slightly distinguishable. Thus, the simplest explanation of the data is that identical complex linear mechanisms operate for both Co(II)-L1 and Zn(II)-L1.

$$E + S \rightleftharpoons ES \longrightarrow (EI_1 \longrightarrow EI_2) \longrightarrow EP \rightleftharpoons E + P$$

Scheme 1: Kinetic Mechanism of L1

The absorption spectrum of uncomplexed Co(II)-substituted-L1 reveals a broad feature at 550 nm with an extinction coefficient of 180 M^{-1} cm^{-1} that we previously assigned to overlapping Co(II) ligand field transitions (48). We examined whether there was a change in the intensities of these ligand field transitions during the reaction of Co(II)-L1 with nitrocefin; however, the presence of the more intense features at 600 and 485 nm

effectively prevented the investigation of any spectral changes due to Co(II) ligand field transitions in the 550 nm region.

Rapid-scanning spectrophotometric studies were also conducted in order to study the reaction of Co(II)-substituted L1 with the other substrates, cephalothin, meropenem, and penicillin G. With these substrates, there were no observed features at 665 or 600 nm, which demonstrates that the chromophoric species observed during the reaction with nitrocefin are due to nitrocefin and its reaction products rather than a chromophoric center in the enzyme. In the absence of interference from absorption due to nitrocefin, Co(II) d-d bands could be observed with the other substrates. However, no significant changes in intensities of these transitions occurred during the reaction, suggesting that there is no change in the coordination number of the Co(II) ions during the time period in which these spectra were obtained (57).

Rapid-Freeze-Quench EPR Spectra of Co(II)-Substituted L1.

The EPR spectrum of Co(II)-substituted L1 is shown in Figure 4A and was simulated (Figure 4B) assuming a single (or two indistinguishable) paramagnetic species with $S = {}^3/_2$, $D \gg \beta g B S$, $M_S = |\pm^1/_2\rangle$, $g_{xy} = 2.32$, $g_z = 2.35$, and $E/D = 0.03$. The origin of an apparently single component EPR signal, which we term the "resting" signal, from the dinuclear Co(II)-containing L1 is a matter for speculation, but the simulation was useful in modeling multicomponent spectra seen under reaction conditions. Variable temperature and power studies were carried out to try to identify other species, but no other Co(II) species were detected between 3.6 and 25 K and at powers up to 200 mW. [The simulation does contain an additional component that we assign to an Fe(III) species and is responsible for the multiple inflection points seen on the derivative feature of the Co(II) signals; this species, with resonances at g-values of 4.74, 3.99, and 3.66, was simulated as Fe(III) with $S = {}^5/_2$, $D \gg \beta g B S$, $g_{iso} = 1.97$, and $E/D = 0.244$. This signal accounted for less than 0.2% of the total spins in the samples and was not investigated further.] Co(II)-substituted L1 was also examined by EPR after reaction with nitrocefin at 2 °C for various times. After 39 ms reaction time, the resting signal was replaced with another apparently single component spectrum (Figure 4E) that we term the "complex" signal. The complex signal was simulated (Figure 4F) assuming $S = {}^3/_2$, $D \gg \beta g B S$, $M_S = |\pm^1/_2\rangle$, $g_{xy} = 2.31$, $g_z = 2.42$, and $E/D = 0.03$. At the shortest reaction time that we could access, 10.4 ms, the spectrum (Figure 4C) could be well modeled (Figure 4D) as a mixture of 15% of the resting signal and 85% of the complex signal. When rapid-freeze-quenched samples were thawed and refrozen after 30 s, an EPR spectrum that consisted of roughly 50% of the resting signal and 50% of the complex signal was observed. This latter spectrum was very similar to the EPR spectrum (Figure 4I) exhibited upon the addition of the hydrolysis product of nitrocefin to Co(II)-substituted L1.
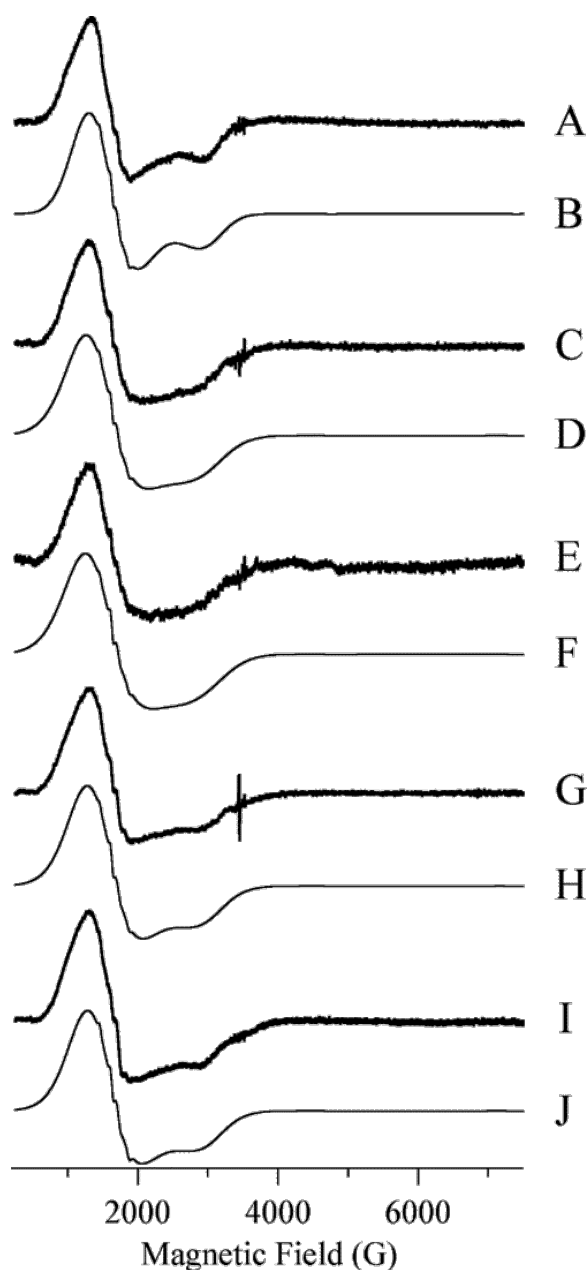
Figure 4 Trace A shows the resting EPR signal of Co(II)-L1. Traces C, E, and G show the EPR spectra of Co(II)-L1 upon reaction with nitrocefin for 10 ms at 2 °C (C), 39 ms at 2 °C (E), and 30 s at 23 °C (G). Trace I shows the EPR spectrum of Co(II)-L1 upon incubation for 5 min at 23 °C with the L1-hydrolyzed product of nitrocefin. Trace B is a computer simulation of (A) assuming $S = {}^3/_2$, $D \gg \beta gBS$ (50 cm^{-1}), $M_S = |\pm^1/_2\rangle$, $g_{xy} = 2.32$, $g_z = 2.35$, and $E/D = 0.03$. Trace F is a computer simulation of (E) assuming $S = {}^3/_2$, $D \gg \beta gBS$ (50 cm^{-1}), $M_S = |\pm^1/_2\rangle$, $g_{xy} = 2.31$, $g_z = 2.42$, and $E/D = 0.03$. Traces B and F also contain a 0.2% minor component due to Fe(III) with $S = {}^5/_2$, $D = 20$ cm^{-1}, $g_{iso} = 1.97$, and $E/D = 0.244$. Traces D, H, and J are models for traces C, G, and I, respectively, and consist of $(0.15 \times B) + (0.85 \times F)$ (D), $(0.50 \times B) + (0.50 \times F)$ (H), and $(0.52 \times B) + (0.48 \times F)$ (J). Experimental EPR spectra were recorded at 12 K with 1 mW microwave power at 9.63 GHz. 10 G (1 mT) field modulation at 100 kHz was employed.

To compare with nitrocefin, analogous experiments were performed using the related cephalosporin cephalothin. After reaction times of 10 and 39 ms, the EPR signals obtained (Figure 5B,C) were indistinguishable from the complex signal that was seen with nitrocefin. However, after thawing a sample and refreezing after 60

s, an entirely new signal was observed (Figure 4D). This signal could be readily simulated (Figure 5E), although g_z was not resolved and all that can reliably be determined from the simulation is that g_{xy} = 2.28 and E/D is low (<0.05). A similar signal was observed (Figure 5F) upon addition of the hydrolysis product of cephalothin (containing no acetate group), though the signal contained a small amount of a second, poorly defined, broad component, estimated as accounting for 20% of the spin density by modeling using the complex signal. Two other substrates were examined by EPR of freeze-quenched samples, meropenem and penicillin G. With meropenem, signals were observed after 10 ms (Figure 6B) and 39 ms (Figure 6D) that were visually distinguishable from the complex signals exhibited upon reaction of Co(II)-substituted L1 with nitrocefin and with cephalothin, but simulation (Figure 6C) showed their EPR parameters to be very similar, with only a slight difference in E/D, 0.05 and 0.03 for meropenem and nitrocefin, respectively. After thawing a sample and refreezing after 60 s, the signal changed slightly (Figure 6E), but a new signal (Figure 6F) was seen upon addition of the hydrolysis product of meropenem to Co(II)-substituted L1. This signal could not be well simulated as either a single species or a mixture of any of the other EPR signals from Co(II)-substituted L1. Somewhat similar behavior was exhibited upon the reaction of Co(II)-substituted L1 with penicillin G. A signal (Figure 7B) was observed after 10 ms that superficially resembled the complex signal, though the simulation (Figure 7C) indicated slightly different parameters of g_{xy} = 2.38, g_z = 2.50, and E/D = 0.005. This signal persisted when the sample was thawed and refrozen after 30 s (Figure 7D), but, as with meropenem, a different signal was observed (Figure 7E) upon adding the hydrolysis product of penicillin G to Co(II)-substituted L1. An attempt to model the spectrum using a mixture of the complex and resting signals was not entirely successful (Figure 7F), and it is likely that new species are involved.

Figure 5 Trace A shows the resting EPR signal of Co(II)-L1. Traces B, C, and D show the EPR spectra of Co(II)-L1 upon reaction with cephalothin for 10 ms at 2 °C (B), 39 ms at 2 °C (C), and 60 s at 23 °C (D). Trace F shows the EPR spectrum of Co(II)-L1 upon incubation for 5 min at 23 °C with the L1-hy-drolyzed product of cephalothin. Trace E is a computer simulation of (D) assuming $S = {}^3/_2$, $D \gg \beta gBS$ (50 cm^{-1}), $M_S = |\pm {}^1/_2\rangle$, $g_{xy} = 2.28$, $g_z = 2.35$, and $E/D = 0.03$. Trace G is a model for trace F and consists of (0.80 × B) + (0.20 × trace F of Figure 4). Trace G also contains a 0.2% minor component due to Fe(III) with $S = {}^5/_2$, $D = 20$ cm^{-1}, $g_{iso} = 1.97$, and $E/D = 0.244$. Experimental EPR spectra were recorded at 12 K with 1 mW microwave power at 9.63 GHz. 10 G (1 mT) field modulation at 100 kHz was employed.
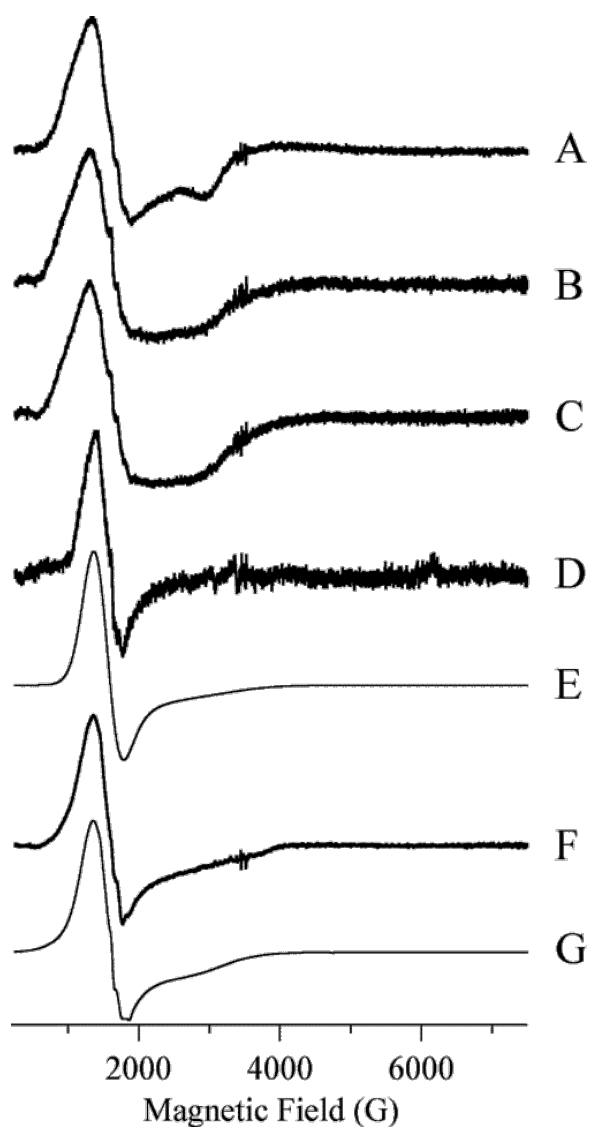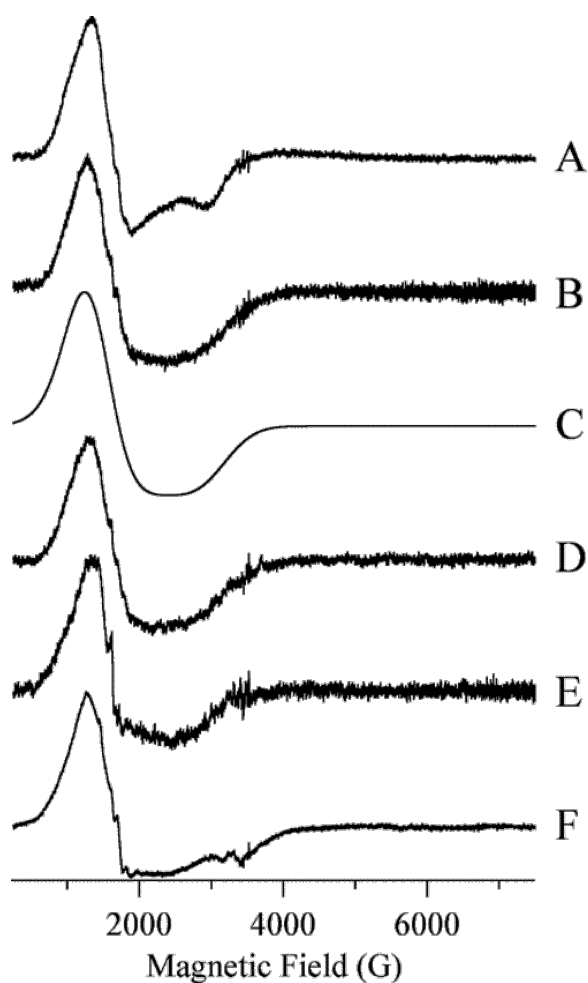
Figure 6 Trace A shows the resting EPR signal of Co(II)-L1. Traces B, D, and E show the EPR spectra of Co(II)-L1 upon reaction with meropenem for 10 ms at 2 °C (B), 39 ms at 2 °C (D), and 60 s at 23 °C (E). Trace F shows the EPR spectrum of Co(II)-L1 upon incubation for 5 min at 23 °C with the L1-hydrolyzed product of meropenem. Trace C is a computer simulation of (B) assuming $S = {}^3/_2$, $D \gg \beta gBS$ (50 cm^{-1}), $M_S = |\pm{}^1/_2\rangle$, $g_{xy} = 2.32$, $g_z = 2.35$, and $E/D = 0.05$. Experimental EPR spectra were recorded at 12 K with 1 mW microwave power at 9.63 GHz. 10 G (1 mT) field modulation at 100 kHz was employed.
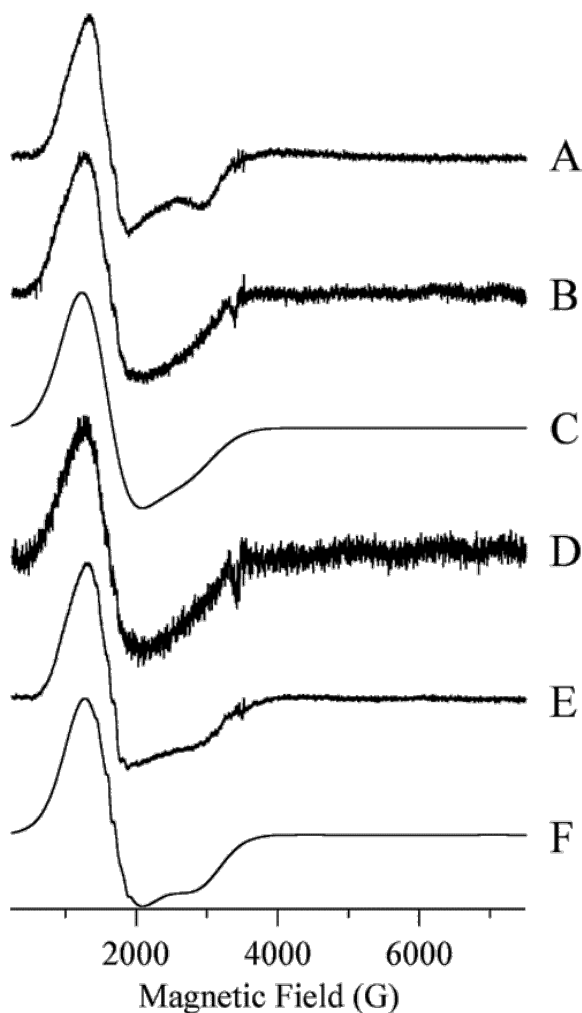
Figure 7 Trace A shows the resting EPR signal of Co(II)-L1. Traces B, D, and E show the EPR spectra of Co(II)-L1 upon reaction with penicillin G for 10 ms at 2 °C (B), 39 ms at 2 °C (D), and 60 s at 23 °C (E). Trace F shows the EPR spectrum of Co(II)-L1 upon incubation for 5 min at 23 °C with the L1-hydrolyzed product of penicillin G. Trace C is a computer simulation of (B) assuming $S = {}^3/_2$, $D \gg \beta gBS$ (50 cm^{-1}), $M_S = |\pm^1/_2\rangle$, $g_{xy} = 2.38$, $g_z = 2.50$, and $E/D = 0.005$. Trace F is a model for trace E and consists of (0.40 × C) + (0.60 × trace B of Figure 4). Trace F also contains a 0.2% minor component due to Fe(III) with $S = {}^5/_2$, $D = 20$ cm^{-1}, $g_{iso} = 1.97$, and $E/D = 0.244$. Experimental EPR spectra were recorded at 12 K with 1 mW microwave power at 9.63 GHz. 10 G (1 mT) field modulation at 100 kHz was employed.

Discussion

Kinetic studies on L1 (*44, 45*) and the related enzymes metallo-β-lactamase CcrA from *B. fragilis* (*43, 46*) and β-lactamase II (*58*) have suggested a common mechanism for the hydrolysis of the chromophoric substrate nitrocefin by these enzymes. The proposed mechanism invokes rapid formation of an intermediate complex, which may involve one or more steps, followed by rate-limiting breakdown of this penultimate species to complete the reaction cycle. Stopped-flow fluorescence studies suggest that the hydrolyses of other substrates of L1, including carbapenems and other cephalosporins, proceed through analogous mechanisms, though the chemical natures of the intermediates may differ in an important respect (*44*). With nitrocefin, it has been proposed that the intermediate whose breakdown is rate-limiting is a ring-opened, anionic species and that this species is stabilized by both interaction with the catalytic site metal ions in L1 and by the presence of a dinitro-substituted styryl substituent that can accommodate excess electron density through the formation of

resonance structures (*43, 46*). However, the available evidence suggests that the β-lactam bond remains intact as the stable intermediate forms when using other β-lactams as substrates (*44*). The breakdown of these intermediates with other substrates must involve hydrolytic cleavage of the β-lactam amide bond, and thus, the mechanism of hydrolysis of nitrocefin may be unique. In the absence of the need for stabilization of a high-energy intermediate, such as the proposed nitrogen anionic species of nitrocefin, it is not immediately clear whether the metal ions would be expected to perform a role in formation of an enzyme–substrate complex. Prior to the present study, no direct evidence for such a role had been presented.

Comparison of the RFQ-EPR and stopped-flow spectrophotometric data for the reaction of Co(II)-substituted L1 with nitrocefin confirmed the earlier proposals that the metal ions are indeed involved in stabilizing the rate-limiting complex. The rate constant of formation of the well-studied 665 nm complex was measured at 54 s^{-1} at 2 °C and that of the appearance of absorbance at 600 nm, not observed with the native Zn(II) enzyme, at 72 s^{-1}. Since the feature at 600 nm occurred only in the time-dependent spectrophotometric studies on Co(II)-substituted L1, and not Zn(II)-containing L1, this feature is obligatorily dependent upon the chemical nature of Co(II); i.e., it must involve the electronic structure of the metal ion. Thus, we can only assign this feature to a Co(II)-bound intermediate species. That we do not see the two distinct intermediates with Zn(II) may be due simply to poorer spectral resolution due to slight differences in the electronic structures of the intermediates, entirely consistent with the intimate involvement of the metal ions in the intermediates. In the case of more extensive spectral overlap in the Zn(II) intermediate, temporal resolution would not be possible because of the similar rate constants of formation (54 versus 72 s^{-1}) and essentially indistinguishable rate constants of decay (7.0 versus 6.7 s^{-1}) of the two intermediates.

The stopped-flow spectrophotometric data indicate that within the shortest reaction time accessible in the RFQ-EPR experiment, 10 ms, significant formation of the enzyme–substrate complex would have occurred. Should the metal ions be involved in the formation of this complex, the consequent perturbation of the electronic structure would be observable in the EPR spectrum. This was, indeed, the case; the EPR data showed that only 15% of the enzyme remained in the resting state after 10 ms and that after 39 ms the resting state, which decayed at a rate constant of 67 s^{-1} in the stopped-flow experiments, was undetectable and only the complex signal remained.

Earlier work (*43–46*) had suggested that the formation of the intermediate with nitrocefin likely involves the metal ions. However, this mechanism may be unique for nitrocefin. There is as yet no clear rationale for the role of metal ions in the formation or stabilization of the intermediate in the proposed closed-ring-intermediate mechanism proposed for the therapeutic antibiotic substrates of L1 (*44*). RFQ-EPR studies were therefore carried out with cephalothin, a nonchromophoric cephalosporin related to nitrocefin but lacking the dinitrostyryl substituent, and, therefore, more strictly analogous to cefaclor, a cephalosporin substrate that has been proposed to form a closed-ring intermediate when reacted with L1 (*44*). After the shortest available reaction time, 10 ms, the resting enzyme signal was completely undetectable, and a signal indistinguishable from the complex signal of Co(II)-L1-nitrocefin was observed. This signal persisted after a 39 ms reaction time. Thus, it is clear that with cephalothin, as with nitrocefin, a perturbation of the electronic structures of one or both of the metal ions occurs in a time consistent with formation of the intermediate. Clearly, then, cephalosporins that are proposed to form both open-ring and closed-ring intermediates interact with the metal center of L1 in doing so.

To further test the generality of the involvement of the metal center of L1 in formation of reaction intermediates, meropenem, a carbapenem, and penicillin G were also examined. Although the literature values of k_{cat} for both meropenem and nitrocefin are reported to vary somewhat depending on precise conditions (*18, 44, 59*), they appear to be generally comparable, whereas the k_{cat} for penicillin G is significantly higher (*34, 49, 50*). As with the cephalosporins, both of these substrates cease to exhibit the resting signal after only very short reaction times, indicative of participation of the metal center in formation of the intermediate.

In addition to providing kinetic information, some structural information can often be derived from EPR of $S = {}^3/_2$ Co(II) (*52*). The axial zero-field splitting, D, is generally sufficiently large that only one of the two Kramers' doublets is thermally populated. Signals from the $M_S = |{\pm}{}^3/_2\rangle$ doublet are effectively diagnostic for tetrahedral-based geometry, whereas signals from the $M_S = |{\pm}{}^1/_2\rangle$ doublet indicate five- or six-coordinate Co(II). The rhombic distortion of the axial zero-field splitting, E/D, where ${}^1/_3 \geq E/D \geq 0$, is a measure of the amount of axial electronic symmetry and thus reflects the symmetry of the ligand field. Further information can be extracted from line width measurements. Co(II) often exhibits broad lines due to extensive strain in **g**, in **A**, and in the zero-field splitting tensor, **D**. These strains are, in turn, due to the freezing out of a continuity of microheterogeneous conformers, afforded by vibrational flexibility and often associated with solvent-derived ligands, such as water or hydroxyl, with poorly defined orientations. On the other hand, the observation of resolved hyperfine structure and very narrow lines indicates a very tightly constrained ligand sphere such as would be provided by polydentate ligands, including rigid proteins.

All of the signals that were observed from Co(II)-L1 were due to transitions in the $M_S = |{\pm}{}^1/_2\rangle$ Kramers' doublet and are due, therefore, to either five- or six-coordinate Co(II). The signals are all essentially axial, with $E/D \leq$ 0.05, and this high degree of axial electronic symmetry is suggestive of an axially symmetric ligand field. The *g*-values for the resting and complex signals are close to those computed for an axially symmetric tetragonal system, where $g_z = 2.43$ and $g_{xy} = 2.50$ (*60*), and support the conclusion that the EPR-detected Co(II) is in an axially symmetric ligand field. The line shapes of the various spectra are more clearly distinct, reflecting different orientational distributions and magnitudes of the strain terms that determine them. The spectra of high-spin Co(II) are dominated by the zero-field splittings, and the line widths are dominated by multiple strain terms in **D** (which includes **E**), **A**, and **g**. Simulation of the spectra is often useful because it provides a value for E/D, a measure of the degree of the electronic axial symmetry. However, there is no unique solution to the spin Hamiltonian unless an axial or isotropic **g** tensor is assumed. Consequently, the kind of detailed information that is available for $S = {}^1/_2$ systems from small anisotropies in **g** is elusive at present for high-spin Co(II) (note that we quote *g*-values to two decimal places, whereas *g*-values can be reliably determined to four decimal places in $S = {}^1/_2$ systems). The often high degree of strain renders superhyperfine structure unresolvable. Thus, high-resolution structural information is often not forthcoming from the EPR of Co(II). However, even subtle changes in the line shape are indicative of substantial changes in the Co(II) coordination environment; indeed, due to the broad lines and relative insensitivity to **g** of the spectra, substantial changes are required in the Co(II) electronic structure if any change in the EPR spectrum is to be observed. Therefore, while detailed structural information from the EPR spectra is not available, the essential point remains that the changes in the EPR spectra upon reaction with substrates, particularly changes in the large strain parameters, are indicative of major changes in the Co(II) environment.

One structural detail that must be considered as a catalytic intermediate is that of a dinuclear metal center that incorporates a substrate moiety in the form of a μ-bridging ligand. In cases where substrates or inhibitors form μ-bridges, the EPR signal is typically lost in antiferromagnetically coupled dicobalt species, or else an integer spin signal may be observed (*61–63*). In the spectra of analogous heterodinuclear Co–Zn systems, very narrow lines are observed with resolved [59]Co hyperfine structure (*52*, *61*, *62*). The exhibition of $S = {}^3/_2$ signals with large line widths in all of the spectra of Co(II)-L1 argues strongly against any of the species containing a substrate-derived μ-bridge bound to both metal ions.

Further information on the catalytic cycle of L1 can be obtained by investigation of the interaction of the hydrolysis products of substrates with the enzyme. With each of the four substrates examined, an EPR signal was obtained upon the addition of product to Co(II)-L1 that was different from both the resting signal and the complex signals obtained at reaction times optimal for generating the intermediate. In the case of nitrocefin and penicillin G, the signals obtained upon adding product to Co(II)-L1 were similar to models generated by adding

proportions of the complex and resting signals, though the model was not a particularly good fit to the data for penicillin G. It is unclear, then, whether any new species are involved or whether the product-bound form of the enzyme is very similar to the intermediate but with a poor binding constant. It is interesting that the spectrum from Co(II)-L1 incubated with penicillin G for 60 s, after which all of the penicillin G would be expected to have been hydrolyzed, gave a spectrum different from that of Co(II)-L1 to which the preprepared hydrolysis product was added. It is possible that, at the very high concentration of reagents being used, substrate inhibition may occur due to transient formation of nonhydrolyzable intermediates. Alternatively, product dissociation and association may be very slow. Although the precise mechanism for the formation of product-related EPR signals is unknown, however, it is clear that there is an interaction of the hydrolysis products of penicillin G and nitrocefin with Co(II)-L1. An EPR signal, which could not be modeled by assuming mixtures of resting and complex signals, was seen upon adding the hydrolysis product of meropenem to Co(II)-L1, though features in the spectra suggest that there is at least some contribution from the resting signal. The effect of adding the hydrolysis product of cephalothin to Co(II)-L1, however, was striking. A new species was observed with atypically narrow g_{xy} features but with g_z so broadened as to be unresolvable. The signal was also seen when cephalothin was allowed to react completely with Co(II)-L1. In the case of cephalothin, then, clear evidence exists for a distinct product complex that is formed in essentially stoichiometric amounts.

The EPR data clearly indicate that the products of hydrolysis interact with the catalytic metal ions of Co(II)-L1 to form significant amounts of an enzyme–product complex. Importantly, previous kinetic simulations on L1 assumed reversible binding of products to the resting enzyme (*45*); the EPR data presented herein support this assumption and emphasize that this step must be included in future kinetic simulations on L1.

Through RFQ-EPR, it has been possible to characterize EPR-detectable Co(II) in Co(II)-L1. Co(II)-L1 contains two Co(II) ions per monomer, presumably in close proximity in a dinuclear active site. However, the EPR spectrum from the resting enzyme can be explained in terms of a single paramagnetic species. Upon reaction with cephalothin for 10–40 ms, the resting signal is converted into the complex signal, which can also be explained in terms of a single paramagnetic species. Finally, upon complete hydrolysis of cephalothin, yet another single species is exhibited in the EPR, corresponding to an enzyme–product complex. In principle, to determine the number of Co(II) ions contributing to the EPR signal, the EPR spectrum can be doubly integrated and the spin concentration calculated. In practice, this can be extremely difficult for high-spin Co(II), particularly for dinuclear systems. The spectral envelope can be extremely wide, 500 mT (5000 G) or more, and even small errors in background subtraction can affect the quantitation significantly. The spectra are also weak in intensity, due to the broad lines and the dilution of the enzyme by a factor of 4 as a consequence of the RFQ procedure, and so contain much noise. Because the spectra are weak, it is often impractical to record spectra under strictly nonsaturating or nonpassage conditions, and integration results are therefore not valid. Finally, in a dinuclear system there is always the possibility, as occurs in VpAP (*53*), that a proportion of the molecules contain a strongly spin-exchange coupled pair of Co(II) ions that exhibit no EPR signal. Quantitation of the signals from Co(II)-L1, therefore, is impracticable. However, some insight into the contributions of the two Co(II) ions to the EPR signal may be available from consideration of the crystal structure of L1 (*35*) and the EPR data. The two Zn ions in L1 are each ligated by three amino acid side chains and are bridged by a solvent-derived oxygen atom (presumably −OH or H_2O). In the case of Zn_1, the amino acids are all histidines, furnishing a four-coordinate site, whereas Zn_2 has two histidines, one aspartate ligand, and a terminal −OH or H_2O. Zn_2, then, has the possibility of being five-coordinate or even six-coordinate. All of the EPR signals observed from Co(II)-L1 can be assigned to either five- or six-coordinate Co(II). Four-coordinate distorted tetrahedral Co(II) gives rise to EPR signals in the $M_S = |\pm^3/_2\rangle$ doublet. However, as the distortion is decreased, $E/D \rightarrow 0$, $g_{xy} \rightarrow 0$, and the transition probability, i.e., the signal intensity, tends to zero. Therefore, for axially symmetric tetrahedral Co(II), the signal is either very weak indeed or nonexistent. Also, $M_S = |\pm^3/_2\rangle$ species of Co(II) are often very fast relaxers; in the case of VpAP in complexation with thiol-based inhibitors, microwave powers of up to 550 mW at 3.6 K were

required to observe $M_S = |\pm^3/_2\rangle$ EPR signals (*64, 65*). It is, then, entirely possible that a tetrahedral site in Co(II)-L1 could go undetected. The electronic absorption spectrum of Co(II)-substituted L1 does indeed indicate the presence of a tetrahedral Co(II) ion; the extinction coefficient of 180 M^{-1} cm^{-1} is too high to be due to two five- or six-coordinate Co(II) ions and, instead, is consistent with a four- and a five- or six-coordinate Co(II) ion (*66*). That we do see clear substrate and product binding to a five- or six-coordinate EPR-detected Co(II) in Co(II)-L1 leads us to propose that Zn$_2$ must play an intimate role in hydrolysis. The role of Zn$_1$ is as yet unclear, though we as yet have no evidence from either EPR or optical spectroscopy for the substrate-induced conversion of a tetrahedral Co(II) to a five- or six-coordinate Co(II) ion during catalysis. The available crystallographic, EPR, and electronic absorption data, then, indicate no clear role for Zn$_1$, and further investigation of Zn$_1$ is clearly warranted.

The use of stopped-flow spectrophotometry and RFQ-EPR has shown that the formation of the intermediate in the reaction of L1 with three classes of β-lactam-containing antibiotics involves binding at one or both of the active site metal ions. This binding occurs at a catalytically competent rate and produces spectroscopically distinct intermediates with different classes of substrate. However, the intermediates generated by nitrocefin and the other substrates are electronically similar, nonetheless, and the intimate involvement of the metal ions in formation and stabilization of the intermediate is general and, therefore, relevant to therapeutically important substrates. A previously unidentified interaction between the reaction products and the metal site of L1 has been characterized, and any full description of the kinetics and mechanism of the reaction must take into account product binding and dissociation. Consideration of the EPR and electronic absorption data, along with crystallographic information (*35*), leads us to propose that Zn$_2$ is intimately involved in the hydrolytic reaction of L1.

References

1 Neu, H. C. (1992) The Crisis in Antibiotic Resistance, *Science257*, 1064−1073.

2 Levy, S. B. (1998) The Challenge of Antibiotic Resistance, *Sci. Am.3*, 47−53.

3 Kotra, L. P., and Mobashery, S. (1999) Mechanistic and Clinical Aspects of β-Lactam Antibiotics and β-Lactamases, *Arch. Immunol. Ther. Exp.47*, 211−216.

4 Bush, K., and Mobashery, S. (1998) in *Resolving the Antibiotic Paradox* (Mobashery, R. A., Ed.) pp 71−98, Kluwer Academic/Plenum Publishers, New York.

5 Knowles, J. R. (1985) Penicillin Resistance: The Chemistry of β-Lactamase Inhibition, *Acc. Chem. Res.18*, 97−104.

6 Page, M. I. (1984) The Mechanisms of Reactions of β-Lactam Antibiotics, *Acc. Chem. Res.17*, 144−151.

7 Siemann, S., Evanoff, D. P., Marrone, L., Clarke, A. J., Viswanatha, T., and Dmitrienko, G. I. (2002) *N*-Arylsulfonyl Hydrazones as Inhibitors of IMP-1 Metallo-β-Lactamase, *Antimicrob. Agents Chemother.46*, 2450−2457.

8 Toney, J. H., Hammond, G. G., Fitzgerald, P. M. D., Sharma, N., Balkovec, J. M., Rouen, G. P., Olson, S. H., Hammond, M. L., Greenlee, M. L., and Gao, Y. D. (2001) Succinic acids as potent inhibitors of plasmid-borne IMP-1 metallo-β-lactamase, *J. Biol. Chem.276*, 31913−31918.

9 Lee, N. L. S., Yuen, K. Y., and Kumana, C. R. (2001) β-Lactam Antibiotic and β-Lactamase Inhibitor Combinations, *J. Am. Med. Assoc.285*, 386−388.

10 Bounaga, S., Galleni, M., Laws, A. P., and Page, M. I. (2001) Cysteinyl Peptide Inhibitors of *Bacillus cereus* Zinc β-Lactamase, *Bioorg. Med. Chem.9*, 503−510.

11 Hammond, G. G., Huber, J. L., Greenlee, M. L., Laub, J. B., Young, K., Silver, L. L., Balkovec, J. M., Pryor, K. D., Wu, J. K., Leiting, B., Pompliano, D. L., and Toney, J. H. (1999) Inhibition of IMP-1 Metallo-β-Lactamase and Sensitization of IMP-1 Producing Bacteria by Thioester Derivatives, *FEMS Microbiol. Lett. 459*, 289−296.

12 Williams, J. D. (1999) β-Lactamases and β-Lactamase Inhibitors, *Int. J. Antimicrob. Agents12* (Suppl. 1), S3−S7.

13 Walter, M. W., Valladares, M. H., Adlington, R. M., Amicosante, G., Baldwin, J. E., Frere, J. M., Galleni, M., Rossolini, G. M., and Schofield, C. J. (1999) Hydroxamate Inhibitors of *Aeromonas hydrophila* AE036 Metallo-β-Lactamase, *Bioorg. Chem.27*, 35−40.

14 Crowder, M. W., and Walsh, T. R. (1999) Metallo-β-Lactamases: Structure and Function, *Res. Signpost3*, 105–132.

15 Bush, K. (2001) New β-Lactamases in Gram-Negative Bacteria: Diversity and Impact on the Selection of Antimicrobial Therapy, *Clin. Infect. Dis.32*, 1085–1090.

16 Rice, L. B., and Bonomo, R. A. (2000) β-Lactamases: Which Ones are Clinically Important?, *Drug Resist. Updates3*, 178–189.

17 Bush, K. (1998) Metallo-β-Lactamases: A Class Apart, *Clin. Infect. Dis.27* (Suppl. 1), S-48–53.

18 Galleni, M., Lamotte-Brasseur, J., Rossolini, G. M., Spencer, J., Dideberg, O., and Frere, J. M. (2001) Standard Numbering Scheme for Class B β-Lactamases, *Antimicrob. Agents Chemother.45*, 660–663.

19 Payne, D. J. (1993) Metallo-β-lactamasesA New Therapeutic Challenge, *J. Med. Microbiol.39*, 93–99.

20 Payne, D. J., Bateson, J. H., Gasson, B. C., Proctor, D., Khushi, T., Farmer, T. H., Tolson, D. A., Bell, D., Skett, P. W., Marshall, A. C., Reid, R., Ghosez, L., Combret, Y., and Marchand-Brynaert, J. (1997) Inhibition of Metallo-β-Lactamases by a Series of Mercaptoacetic Acid Thiol Ester Derivatives, *Antimicrob. Agents Chemother.41*, 135–140.

21 Payne, D. J., Bateson, J. H., Gasson, B. C., Khushi, T., Proctor, D., Pearson, S. C., and Reid, R. (1997) Inhibition of Metallo-β-Lactamases by a Series of Thiol Ester Derivatives of Mercaptophenylacetic Acid, *FEMS Microbiol. Lett. 157*, 171–175.

22 Yang, K. W., and Crowder, M. W. (1999) Inhibition Studies on the Metallo-β-Lactamase L1 from *Stenotrophomonas maltophilia*, *Arch. Biochem. Biophys. 368*, 1–6.

23 Felici, A., Perilli, M., Segatore, B., Franceschini, N., Setacci, D., Oratore, A., Stefani, S., Galleni, M., and Amicosante, G. (1995) Interactions of Biapenem with Active Site Serine and Metallo-β-Lactamases, *Antimicrob. AgentsChemother.39*, 1300–1305.

24 Prosperi-Meys, C., Llabres, G., de Seny, D., Soto, R. P., Valladares, M. H., Laraki, N., Frere, J. M., and Galleni, M. (1999) Interaction between Class B β-Lactamases and Suicide Substrates of Active-Site Serine β-Lactamases, *FEBS Lett.443*, 109–111.

25 Nagano, R., Adachi, Y., Imamura, H., Yamada, K., Hashizume, T., and Morishima, H. (1999) Carbapenem Derivatives as Potential Inhibitors of Various β-Lacamases, Including Class B Metallo-β-Lactamases, *Antimicrob. Agents Chemother.43*, 2497–2503.

26 Toney, J. H., Cleary, K. A., Hammond, G. G., Yuan, X., May, W. J., Hutchins, S. M., Ashton, W. T., and Vanderwall, D. E. (1999) Structure−Activity Relationships of Biphenyl Tetrazoles as Metallo-β-Lactamase Inhibitors, *Bioorg. Med. Chem. Lett.9*, 2741–2746.

27 Arakawa, Y., Shibata, N., Shibayama, K., Kurokawa, H., Yagi, T., Fujiwara, H., and Goto, M. (2000) Convenient Test for Screening Metallo-β-Lactamase Producing Gram Negative Bacteria by Using Thiol Compounds, *J. Clin. Microbiol.38*, 40–43.

28 Khardori, N., Elting, L., Wong, E., Schable, B., and Bodey, G. P. (1990) Nosocomial Infections Due to *Xanthomonas maltophilia* in Patients with Cancer, *Rev. Infect. Dis.12*, 997–1003.

29 Muder, R. R., Yu, V. L., Dummer, J. S., Vinson, C., and Lumish, R. M. (1987) Infections Caused by *Pseudomonas maltophilia*, *Arch. Intern. Med.147*, 1672–1674.

30 Villarino, M. E., Stevens, L. E., Schable, B., Mayers, G., Miller, J. M., Burke, J. P., and Jarvis, W. R. (1992) Risk Factors for Epidemic *Xanthomonas maltophilia* Infection/Colonization in Intensive Care Unit Patients, *Infect. Control Hosp. Epidemiol. 13*, 201–206.

31 Mett, H., Rosta, S., Schacher, B., and Frei, R. (1988) Outer Membrane Permeability and β-lactamase Content in *Pseudomonas maltophilia* Clinical Isolates and Laboratory Mutants, *Rev. Infect. Dis. 10*, 765–819.

32 Walsh, T. R., Payne, D. J., Neville, T., Tolson, D., MacGowan, A. P., and Bennett, P. M. (1997) Sequence Analysis and Kinetics of the Cloned L2 Serine β-Lactamase from *Stenotrophomonas maltophilia*, *Antimicrob. Agents Chemother.41*, 1460–1462.

33 Walsh, T. R., Hall, L., Assinder, S. J., Nichols, W. W., Cartwright, S. J., MacGowan, A. P., and Bennett, P. M. (1994) Sequence Analysis of the L1 Metallo-β-Lactamase from *Xanthomonas maltophilia*, *Biochim. Biophys. Acta1218*, 199–201.

34 Crowder, M. W., Walsh, T. R., Banovic, L., Pettit, M., and Spencer, J. (1998) Overexpression, Purification, and Characterization of the Cloned Metallo-β-Lactamase L1 from *Stenotrophomonas maltophilia*, *Antimicrob. Agents Chemother.42*, 921–926.

35 Ullah, J. H., Walsh, T. R., Taylor, I. A., Emery, D. C., Verma, C. S., Gamblin, S. J., and Spencer, J. (1998) The crystal structure of the L1 metallo-β-lactamase from *Stenotrophomonas maltophilia* at 1.7 angstrom resolution, *J. Mol. Biol.284*, 125–136.

36 Carfi, A., Paul-Soto, R., Martin, L., Petillot, Y., Frere, J. M., and Dideberg, O. (1997) Purification, Crystallization, and Preliminary X-ray Analysis of *Bacteroides fragilis* Zn^{2+} β-Lactamase, *Acta Crystallogr.D53*, 485–487.

37 Bernstein, N. J., and Pratt, R. F. (1999) On the Importance of a Methyl Group in β-Lactamase Evolution: Free Energy Profiles and Molecular Modeling, *Biochemistry38*, 10499–10510.

38 Diaz, N., Suarez, D., and Merz, K. M. (2000) Zinc Metallo-β-Lactamase from *Bacteroides fragilis*: A Quantum Chemical Study on Model Systems of the Active Site, *J. Am. Chem. Soc.122*, 4197–4208.

39 Caselli, E., Powers, R. A., Blasczcak, L. C., Wu, C. Y. E., Prati, F., and Shoichet, B. K. (2000) Energetic, Structural, and Antimicrobial Analyses of β-Lactam Side Chain Recognition by β-Lactamases, *Chem. Biol.49*, 1–16.

40 Suarez, D., and Merz, K. M. (2001) Molecular Dynamics Simulations of the Mononuclear Zinc-β-Lactamase from *Bacillus cereus*, *J. Am. Chem. Soc.123*, 3759–3770.

41 Concha, N. O., Rasmussen, B. A., Bush, K., and Herzberg, O. (1996) Crystal Structure of the Wide-Spectrum Binuclear Zinc β-Lactamase from *Bacteroides fragilis*, *Structure4*, 823–836.

42 Salsbury, F. R., Crowley, M. F., and Brooks, C. L. (2001) Modeling of the Metallo-β-lactamase from *B-fragilis*: Structural and Dynamic Effects of Inhibitor Binding, *Proteins: Struct., Funct., Genet.44*, 448–459.

43 Wang, Z., Fast, W., and Benkovic, S. J. (1999) On the Mechanism of the Metallo-β-Lactamase from *Bacteroides fragilis*, *Biochemistry38*, 10013–10023.

44 Spencer, J., Clark, A. R., and Walsh, T. R. (2001) Novel Mechanism of Hydrolysis of Therapeutic β-Lactams by *Stenotrophomonas maltophilia* L1 Metallo-β-Lactamase, *J. Biol. Chem.276*, 33638–33644.

45 McMannus-Munoz, S., and Crowder, M. W. (1999) Kinetic Mechanism of Metallo-β-Lactamase L1 from *Stenotrophomonas maltophilia*, *Biochemistry38*, 1547–1553.

46 Wang, Z., Fast, W., and Benkovic, S. J. (1998) Direct Observation of an Enzyme-Bound Intermediate in the Catalytic Cycle of the Metallo-β-Lactamase from *Bacteroides fragilis*, *J. Am. Chem. Soc.120*, 10788.

47 Sambrook, J., Fritsch, E. F., and Maniatis, T. (1989) *Molecular Cloning, A Laboratory Manual*, Vol. 1, 2nd ed., Cold Spring Harbor Laboratory Press, Cold Spring Harbor, NY.

48 Crowder, M. W., Yang, K. W., Carenbauer, A. L., Periyannan, G., Seifert, M. A., Rude, N. E., and Walsh, T. R. (2001) The Problem of a Solvent Exposable Disulfide when Preparing 1087 Co(II)-Substituted Metallo-β-Lactamase L1 from *Stenotrophomonas maltophilia*, *J. Biol. Inorg. Chem.6*, 91–99.

49 Carenbauer, A. L., Garrity, J. A., Periyannan, G., Yates, R. B., and Crowder, M. W. (2002) Probing Substrate Binding to Metallo-β-Lactamase L1 from *Stenotrophomonas maltophilia* by Using Site-Directed Mutagenesis, *BMC Biochem.3*, 4–10.

50 Garrity, J. D., Carenbauer, A. L., Herron, L. R., and Crowder, M. W. (2004) Metal Binding Asp-120 in Metallo-β-lactamase L1 from *Stenotrophomonas maltophilia* Plays a Crucial Role in Catalysis, *J. Biol. Chem.279*, 920–927.

51 Wang, D. M., and Hanson, G. R. (1995) A New Method for Simulating Randomly Oriented Powder Spectra in Magnetic-Resonancethe Sydney-Opera-House (Sophe) Method, *J. Magn. Reson. A117*, 1–8.

52 Bennett, B. (2002) EPR of Co(II) as a Structural and Mechanistic Probe of Metalloprotein Active Sites: Characterization of an Aminopeptidase, *Curr. Top. Biophys.26*, 49–57.

53 Bennett, B., and Holz, R. C. (1997) EPR Studies on the Mono- and Dicobalt(II)-Substituted Forms of the Aminopeptidase from *Aeromonas proteolytica*. Insight into the Catalytic Mechanism of Dinuclear Hydrolases, *J. Am. Chem. Soc.119*, 1923–1933.

54 Bennett, B., and Holz, R. C. (1997) Spectroscopically Distinct Cobalt(II) Sites in Heterodimetallic Forms of the Aminopeptidase from *Aeromonas proteolytica*: Characterization of Substrate Binding, *Biochemistry36*, 9837–9846.

55 Bicknell, R., Schaffer, A., Waley, S. G., and Auld, D. S. (1986) Changes in the Coordination Geometry of the Active Site Metal during Catalysis of Benzylpenicillin Hydrolysis by *Bacillus cereus* β-Lactamase II, *Biochemistry25*, 7208−7215.

56 Bicknell, R., and Waley, S. G. (1985) Cryoenzymology of *Bacillus cereus* β-Lactamase II, *Biochemistry24*, 6876−6887.

57 Garmer, D. R., and Krauss, M. (1993) Ab Initio Quantum Chemical Study of the Cobalt d−d Spectroscopy of Several Substituted Zinc Enzymes, *J. Am. Chem. Soc.115*, 10247−10257.

58 Rasia, R. M., and Vila, A. J. (2003) Mechanistic study of the hydrolysis of nitrocefin mediated by *B. cereus* metallo-β-lactamase, *ARKIVOC3*, 507−516.

59 Bicknell, R., Emanuel, E. L., Gagnon, J., and Waley, S. G. (1985) The Production and Molecular Properties of the Zinc β-Lactamase of *Pseudomonas maltophilia* IID 1275, *Biochem. J.229*, 791−797.

60 Lohr, L. L., Miller, J. C., and Sharp, R. R. (1999) Electronic structure and magnetic properties of high-spin octahedral Co(II) complexes: Co(II)(acac)$_2$(H$_2$O)$_2$, *J. Chem. Phys.111*, 10148−10158.

61 Stamper, C., Bennett, B., Edwards, T., Holz, R. C., Ringe, D., and Petsko, C. (2001) Inhibition of the Aminopeptidase from *Aeromonas proteolytica* by *L*-Leucinephosphonic acid. Spectroscopic and Crystallographic Characterization of the Transition State of Peptide Hydrolysis, *Biochemistry40*, 7035−7046.

62 Bennett, B., and Holz, R. C. (1998) Inhibition of the Aminopeptidase from *Aeromonas proteolytica* by *L*-Leucinephosphonic Acid, a Transition State Analogue of Peptide Hydrolysis, *J. Am. Chem. Soc.120*, 12139−12140.

63 Stamper, C. C., Bienvenue, D. L., Bennett, B., Ringe, D., Petsko, G. A., and Holz, R. C. (2004) Spectroscopic and X-ray Crystallographic Characterization of Bestatin Bound to the Aminopeptidase from *Aeromonas (Vibrio) proteolytica*, *Biochemistry43*, 9620−9628.

64 Bienvenue, D. L., Bennett, B., and Holz, R. C. (2000) Inhibition of the Aminopeptidase from *Aeromonas proteolytica* by *L*-Leucinethiol: Kinetic and Spectroscopic Characterization of a Slow, Tight-Binding Inhibitor-Enzyme Complex, *J. Inorg. Biochem.78*, 43−54.

65 Huntington, K. M., Bienvenue, D. L., Wei, Y. M., Bennett, B., Holz, R. C., and Pei, D. H. (1999) Slow-Binding Inhibition of the Aminopeptidase from *Aeromonas* Proteolytica by Peptide Thiols: Synthesis and Spectroscopic Characterization, *Biochemistry38*, 15587−15596.

66 de Seny, D., Heinz, U., Wommer, S., Kiefer, M., Meyer-Klaucke, W., Galleni, M., Frere, J. M., Bauer, R., and Adolph, H. W. (2001) Metal Ion Binding and Coordination Geometry for Wild Type and Mutants of Metallo-β-lactamase from *Bacillus cereus* 569/H/9 (BcII)A Combined Thermodynamic, Kinetic, and Spectroscopic Approach, *J. Biol. Chem.276*, 45065−45078.

1 Abbreviations: EPR, electron paramagnetic resonance; HEPES, 4-(2-hydroxyethyl)-1-piperazineethanesulfonic acid; IPTG, isopropyl β-thiogalactoside; L1, metallo-β-lactamase from *Stenotrophomonas maltophilia*; RFQ, rapid-freeze-quench; SDS−PAGE, sodium dodecyl sulfate−polyacrylamide gel electrophoresis.